EES Solar

PAPER

View Article Online
View Journal | View Issue

Cite this: *EES Sol.*, 2026, **2**, 448

Performance limiting defect stabilization by orbital hybridization in perovskite/C_{60} based solar cells

Richard Gundermann, *[ab] Guorui He, [a] Christopher Penschke, [b] Eros Radicchi, [c] Edoardo Mosconi,[de] Filippo De Angelis,[fdg] Dieter Neher [a] and Felix Lang *[a]

Metal halide perovskites have emerged as promising materials for solar cells, with efficiencies close to silicon. However, trap-assisted nonradiative recombination remains one of the limiting factors, particularly at the interface with the electron transport layer, which employs fullerenes such as C_{60}. In this work, surface defects of tetragonal $CH_3NH_3PbI_3$ ($MAPbI_3$) are investigated in the presence of C_{60}, using hybrid density functional theory (DFT). We found that the presence of C_{60} on the $MAPbI_3$ surface reduces the defect formation energies of certain defects and thereby increases the defect density, in line with previous experimental work [J. Warby *et al.*, *Advanced Energy Materials*, 2022, **12**, 2103567]. Further investigations attribute these results to a hybridization between defects and C_{60} orbitals. This leads to a new understanding of this particular interface and highlights possible strategies to circumvent performance limitations in future perovskite solar cells.

Received 29th September 2025
Accepted 14th January 2026

DOI: 10.1039/d5el00161g

rsc.li/EESSolar

Broader context

Perovskite single and multi-junction solar cells have reached impressive efficiencies rivaling established technologies. However, many single, and the majority of multi-junction, architectures utilize fullerenes (C_{60}) as electron transport layers. With improving bulk perovskite qualities, this layer, currently without alternatives, however, leads to interfacial performance losses of up to 25%rel. Although strong photoluminescence quenching and open-circuit voltage (V_{OC}) degradation are widely observed, the underlying mechanism has remained unclear until now. This knowledge gap hampers progress toward high efficiency single and especially multijunction perovskite photovoltaics. In this work, we uncover a mechanism in which orbital hybridization leads to more surface defects, explaining these limitations and thus we provide a clear target for future interface engineering to unlock the full potential of perovskite solar cells.

1. Introduction

Metal halide perovskites have emerged as promising materials for solar cells, combining simple wet-chemistry fabrication with record efficiencies at 27% close to silicon.[1] Combining a wide band gap perovskite with a low band gap perovskite or silicon in a tandem solar cell further allows for efficiencies exceeding 30.1%/34.9%, respectively.[1]

However, trap-assisted non-radiative recombination at the interfaces between perovskites and adjacent charge transport layers remains one of the limiting factors in perovskite solar cells (PSCs). This is especially problematic in p–i–n type PSCs, which are commonly used in tandem architectures with silicon or perovskite. Recently, we quantified the impact of these interface recombination losses by comparing the measured efficiencies of complete devices with the implied efficiencies of bare absorbers, *i.e.*, without charge transport layers. For perovskite single-junction, perovskite/perovskite and perovskite/silicon tandem solar cells, these interface losses amount to 25%rel, 14%rel, and 19%rel, respectively,[2–4] highlighting interfacial recombination as the primary limitation of current perovskite technologies. In p–i–n type PSCs, these losses are dominated by the perovskite/electron transport layer (ETL) interface, which utilizes the C_{60}-fullerene in the majority of studies.[2–4] Measuring the photoluminescence quantum yield (PLQY) of bare glass perovskite stacks with and without C_{60} reveals a decrease in PLQY by 1–3 orders of magnitude for most of the perovskite compositions, implying a reduced power

[a]*University of Potsdam, Institute of Physics and Astronomy, Karl-Liebknecht-str.24-25, 14476 Potsdam-Golm, Germany. E-mail: gundermann1@uni-potsdam.de; felix.lang.1@uni-potsdam.de*

[b]*University of Potsdam, Institute of Chemistry, Karl-Liebknecht-str.24-25, 14476 Potsdam-Golm, Germany*

[c]*Department of Engineering DIMI, University of Verona, Strada Le Grazie 15, 37134 Verona, Italy*

[d]*Computational Laboratory for Hybrid/Organic Photovoltaics (CLHYO), Istituto CNR di Scienze e Tecnologie Chimiche "Giulio Natta" (CNR-SCITEC), Via Elce di Sotto 8, Perugia, 06123, Italy*

[e]*Chemistry Department, College of Science, King Saud University, Riyadh, 11451, Saudi Arabia*

[f]*Department of Chemistry, Biology and Biotechnology, University of Perugia, Via Elce di Sotto 8, Perugia, 06123, Italy*

[g]*SKKU Institute of Energy Science and Technology (SIEST), Sungkyunkwan University, Suwon 440-746, South Korea*

conversion efficiency (PCE) for a full working device, as shown by Warby *et al.*[5] Interestingly, detailed experiments reveal a relationship between C_{60} surface coverage and PLQY and just a 1 nm thick layer of C_{60} is enough to completely cover the entire perovskite surface, yielding the same PLQY reductions. This suggests a microscopic origin.[5]

Many origins have been proposed to explain this phenomenon, for example, charge transfer states, packing faults of C_{60} or inhomogeneous electrostatics at the surface, which can broaden the density of states (DOS) and pin the lowest unoccupied molecular orbital (LUMO) of C_{60} below the conduction band of the perovskite. This low-lying LUMO was thought to potentially introduce trap states and thus increase non-radiative recombination. Sensitive external quantum efficiency (EQE) measurements revealed subgap states induced by C_{60},[5] supporting this suggestion. However, until today no specific mechanism has been proposed to explain how the presence of the C_{60} ETL could introduce additional traps at the interface of the perovskite. First principles calculations involving a slab-model incorporating $MAPbI_3$ and C_{60} have shown no formation of mid-gap states.[5] As the authors in ref. 5 admit, this was in contradiction to their sensitive EQE measurements.

For a long time, it was assumed that no chemical bond would be created between C_{60} and perovskite, which was argued to be reasonable because of the closed shell nature of C_{60}.[5] In this work, we propose another mechanism, in which the C_{60} will be chemisorbed at defect orbitals, leading to hybridization with the C_{60} LUMO. This stabilizes surface defects, resulting in a lower formation energy and, consequently, higher surface trap densities.

Utilizing drift-diffusion simulations we consequently showed that this result explains the substantial surface recombination at the perovskite/C_{60} interface with the vast V_{OC} losses and PLQY quenching, reported in ref. 5.

2. Methods and models

In this work, we performed density functional theory (DFT) calculations including dispersion corrections (DFT-D3). For most of the work, we employed the PBE functional while for selected cases we also performed calculations with the computationally more expensive HSE functionals, including spin orbit coupling (SOC). The calculations are performed with VASP (5.4.4).[6] More details are provided in the SI.

We construct three exemplary slab-models, incorporating $MAPbI_3$ with a defect at its surface and a single C_{60}. To the best of our knowledge, this is done for the very first time, while recent studies either incorporate a pristine perovskite with C_{60} (ref. 5 and 7) or a perovskite defective at the surface, without C_{60}.[8–10]

In detail, we utilize the tetragonal phase of $MAPbI_3$, which is well known to be stable at room temperature (see *e.g.* ref. 11), and confine ourselves to the most probable (001) surface, following Haruyama *et al.*[8] The slab-model is created by repeating this bulk by $2 \times 2 \times 2$ and adding a vacuum region of ~50%. Each slab used in this work has the dimensions $a = b = 17.711$ Å, $c = 50$ Å, regardless of further details as defects or C_{60}.

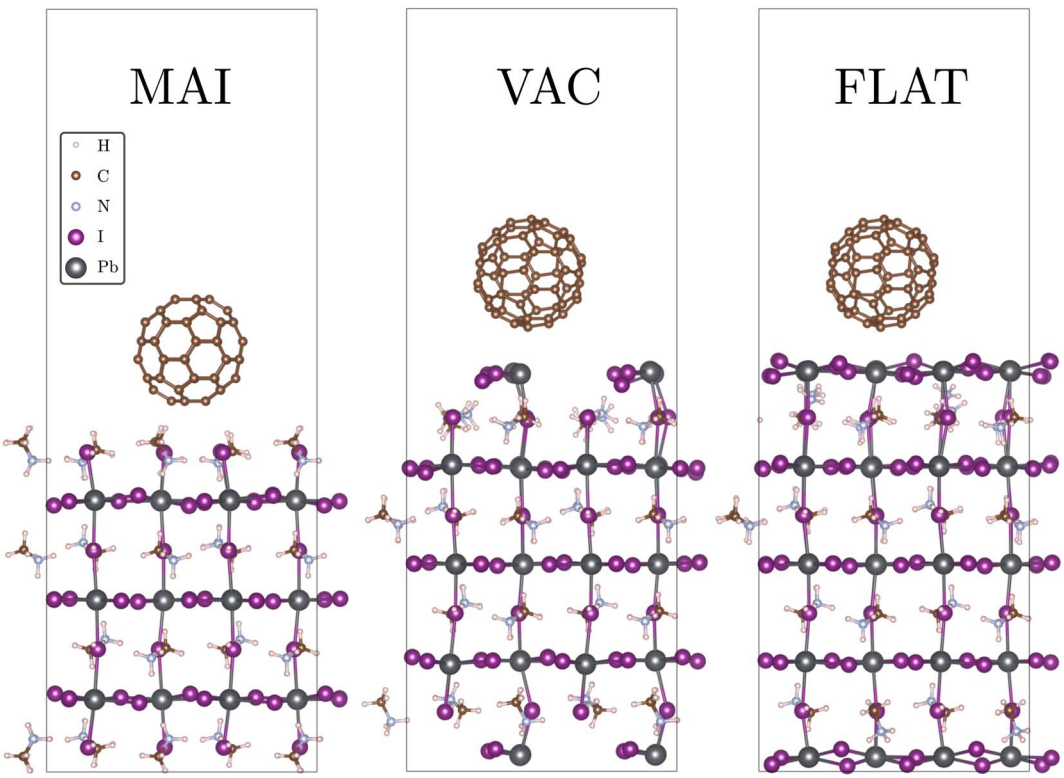

Fig. 1 Slab-models with different surface terminations, following ref. 12. We show methylammonium–iodide (MAI), lead–iodide (FLAT), and vacant (VAC) terminations. The latter can be understood as the intermediate case. In this work, only MAI and VAC are used.

For the (001) surface we considered three different surface terminations, *i.e.* MAI, FLAT and VAC, introduced in Fig. 1, following ref. 9. The MAI termination represents the case with an outermost CH_3NH_3I layer, FLAT an outermost PbI_2 layer, while the VAC termination represents a "vacant" intermediate case formed by eliminating eight PbI_2 units from the FLAT termination.

Next, we added a single C_{60}-molecule in an "aboveBridge" position (MAI-termination) and in an "abovePb" position (VAC and FLAT termination), which are shown to have the largest adsorption energy.[7] Repeating ionic relaxation leads us to Fig. 1. In the next step, we introduced three point defects: a lead interstitial at the MAI terminated surface, denoted by MAI:Pb_i, an iodine interstitial and an iodine vacancy, both at the VAC terminated surface, denoted as VAC:I_i and VAC:V_I, as shown in Fig. 2. More possible point defects at the surface are shown in ref. 9, however we need to restrict our work due to higher computational costs. Our selected point defects lie relatively midgap and thus are suited to act as traps. It is important to emphasize that the C_{60} position is chosen close to the defect. Due to the proximity to the defect, we can observe possible impacts of the presence of C_{60} particularly well. This will be later justified since the adsorption energy will be higher when C_{60} is closer to a defect.

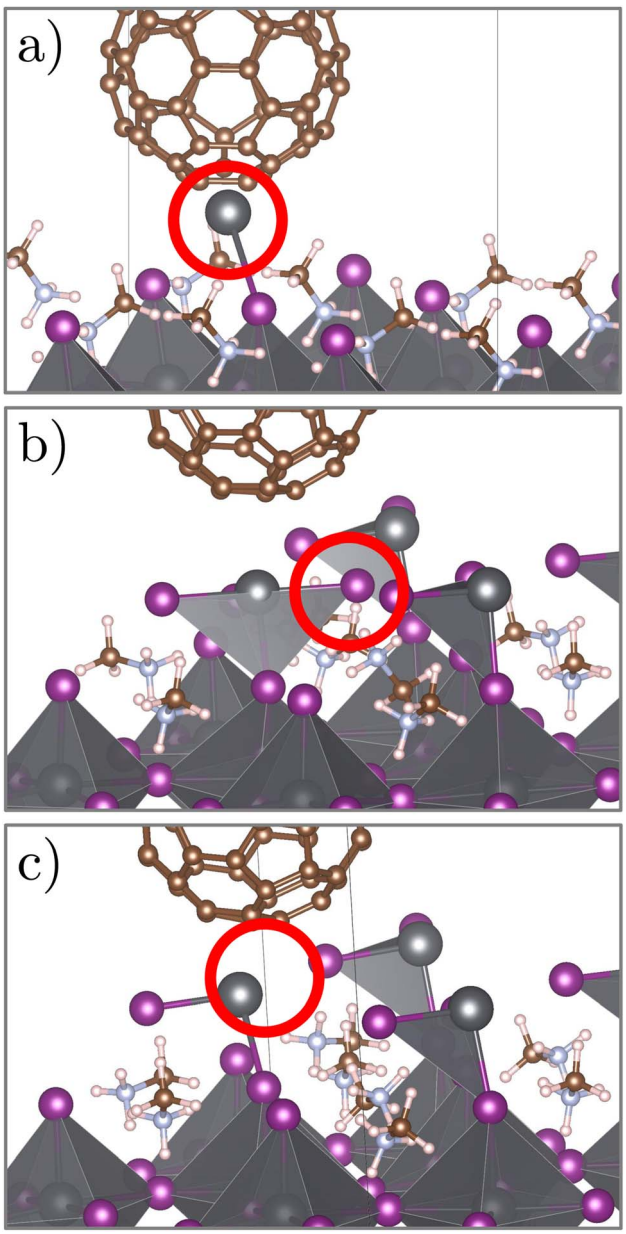

Fig. 2 Insights of slab-models, including the MAI:Pb_i defect (a), VAC:I_i (b) and VAC:V_I (c). The C_{60} molecule is located in the proximity of the defects.

In order to investigate possible stabilization mechanisms of defects due to C_{60}, we introduce the trap density[13] estimated by

$$N_T = N_0 \exp\left\{-\frac{\mathrm{DFE}}{k_B T}\right\} \quad (1)$$

with Boltzmann constant k_B, temperature T (300 K) and a density N_0 of possible lattice sites, to place the defects, and the defect formation energy (DFE). The difference in DFE with and without C_{60} in their proximity gives us a defect stabilization energy (DSE), from which we can calculate the relative change in trap density. As we show in SI chapter IVC3, the difference in DFEs, with or without C_{60}, is equivalent to the difference in adsorption energies of C_{60} with or without the presence of defects.

$$\mathrm{DSE} = E_{\mathrm{ads}}^{\mathrm{prist.}} - E_{\mathrm{ads}}^{\mathrm{def.}} \quad (2)$$

In contrast to DFEs, which include a chemical potential of the point defect species that depend on possible existing secondary phases, adsorption energies can be calculated readily using DFT. Calculating adsorption energies instead of DFEs, we are thus left with a much simpler procedure.

3. Results and discussion

3.1. Defect stabilization

The calculated DSE at the PBE-level is shown for all three cases in Table 1. Corresponding adsorption energies are shown in SI Table 1. One observes a stabilization of ~0.7 eV for MAI:Pb_i and VAC:V_I. On the other hand, VAC:I_i shows no significant stabilization. Considering the dispersion (DFT-D3) contributions of the DSE, these stabilizations originate not only from the

Table 1 Defect stabilization energies (in eV) at PBE and HSE levels and their contribution from dispersion (DFT-D3). The structures of PBE and HSE cases are identical

System	DSE	$\mathrm{DSE}^{\mathrm{disp}}$
PBE		
MAI:Pb_i	0.67	0.18
VAC:I_i	0.04	0.15
VAC:V_I	0.66	0.07
HSE		
VAC:I_i	−0.14	0.15
VAC:V_I	0.16	0.07

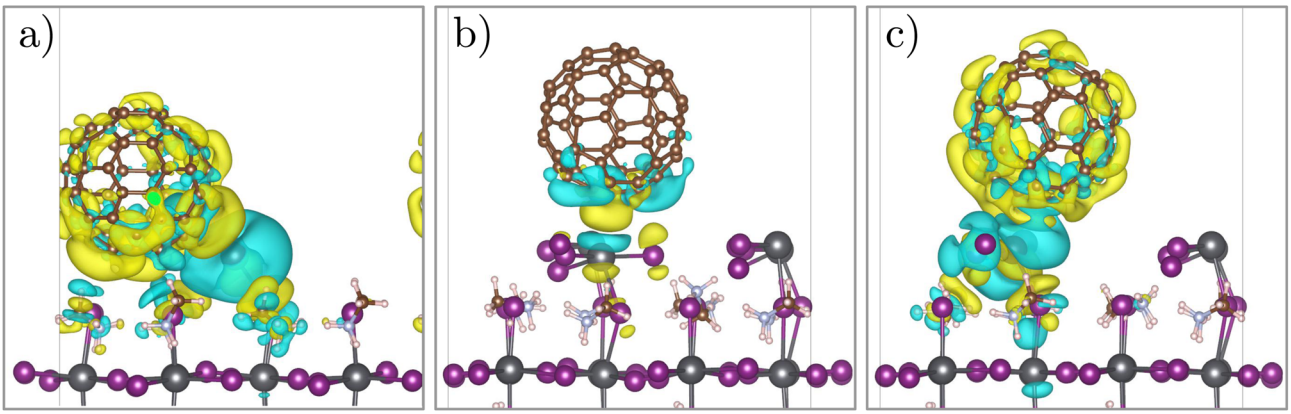

Fig. 3 Valence-electron charge density differences for (a) MAI:Pb_i, (b) VAC:I_i and (c) VAC:V_I at the PBE-level. Yellow isosurfaces correspond to electron enriched regions, and blue to depleted regions. All isosurfaces are plotted at 2.3×10^{-4} e/Bohr^3. Cases (a) and (c) show enriched regions at C_{60} and depleted at the defect.

dispersion, but also largely from an additional mechanism, which we identify as orbital hybridization.

These results can be verified at the computationally more expensive HSE-level, shown in Table 1, where we calculated only VAC:I_i and VAC:V_I, because of computational cost. Again, the latter is stabilized and the former not, confirming our results. Corresponding adsorption energies are provided in SI Table 2, as well as partial density of states and orbitals in SI chapters III and VI.

Besides the fact that only two defects show stabilization and that the number of defect types and positions is restricted due to computational costs, these results have important consequences for the observations in Warby *et al.*[5] According to eqn (1), the surface trap density for a DSE of 0.67 eV increases by eleven orders of magnitude. At the HSE-level, a smaller DSE of 0.16 eV remains for the VAC:V_I, but still sufficient to increase the surface trap density by two to three orders of magnitude, influencing the PLQY as observed in their experiments. Since this stabilization is induced by C_{60} in the proximity of the surface defects, their observed dependence on surface coverage can be explained. Furthermore, our results possibly explain the observed subgap states, induced by C_{60}, reported in the same work by using sensitive EQE measurements.

Exploring the mechanism of this stabilization trend is of great interest for improving future perovskite-based single and tandem solar cells.[2–4] We start our investigation by showing valence-electron charge density differences for all three cases in Fig. 3, see SI chapter IVC for a precise definition. For (a) and (c) one observes the C_{60} as an electron enriched region and the defects as depleted. A stabilization of the defect and/or C_{60} is therefore qualitatively clarified by electrostatic attraction. Case (b) shows a slight charge redistribution, but significantly smaller than (a) and (c). This is in line with our previous trend of DSE values. Notice that this redistribution can be understood as chemisorption.

One could now question the origin of these charge redistributions. In SI IVC4 we present an extended discussion that this redistribution can be either attributed to different orbital occupation numbers in the combined system or to hybridization of C_{60} and defect orbitals. We investigated the latter possibility by showing wavefunctions, associated with the defect level in Fig. 4. Comparing the cases with and without C_{60}, we indeed observe a hybridization of the C_{60}-LUMO and the defect orbital, except for the VAC:I_i, which is again in line with our trend of DSE values. A complete overview of wavefunctions can be found in SI chapter VI.

If one still tries to find a possible reason why VAC:I_i exhibits no hybridization, this can be illustrated using electron counting. The lead atom usually supplies two electrons in total (as p-orbital) to its two in-plane iodine neighbors because of the higher electronegativity. As seen in Fig. 2, those two neighbors do not exist for MAI:Pb_i and VAC:V_I. Instead, the lead supplies its electrons partially to the C_{60}. In the case of VAC:I_i one of the lead atoms has even three neighbors. Otherwise, the iodine atom cannot supply its electrons to the C_{60} for electronegativity reasons.

As discussed in standard textbooks of molecular orbital theory, orbital hybridization is mainly caused by a large overlap of two neighboring orbitals, influenced by shape, distance and orientation, as well as a small difference in the orbital energy level. We repeated our calculation at the HSE-level, which possibly changes the positions of energy levels and the emergence of hybridization. However, an increased DSE in the presence of C_{60} was already found in Table 1 and indeed, we found hybridization again. Respective wavefunctions in SI chapter VI show hybridization for VAC:V_I and not for VAC:I_i, in line with our previous results. A partial density of states plot can be found in SI chapter III.

To conclude this part of the paper, our DFT calculations predict the stabilization of certain defects at the perovskite surface in the presence of C_{60} molecules, in line with the observations of Warby *et al.*[5] We also identify the role of orbital hybridization as the microscopic origin.

3.2. Impact on recombination

To show the relative impact of the increased surface trap densities on the PLQY and thus Quasi-Fermi-Level Splitting (QFLS) and

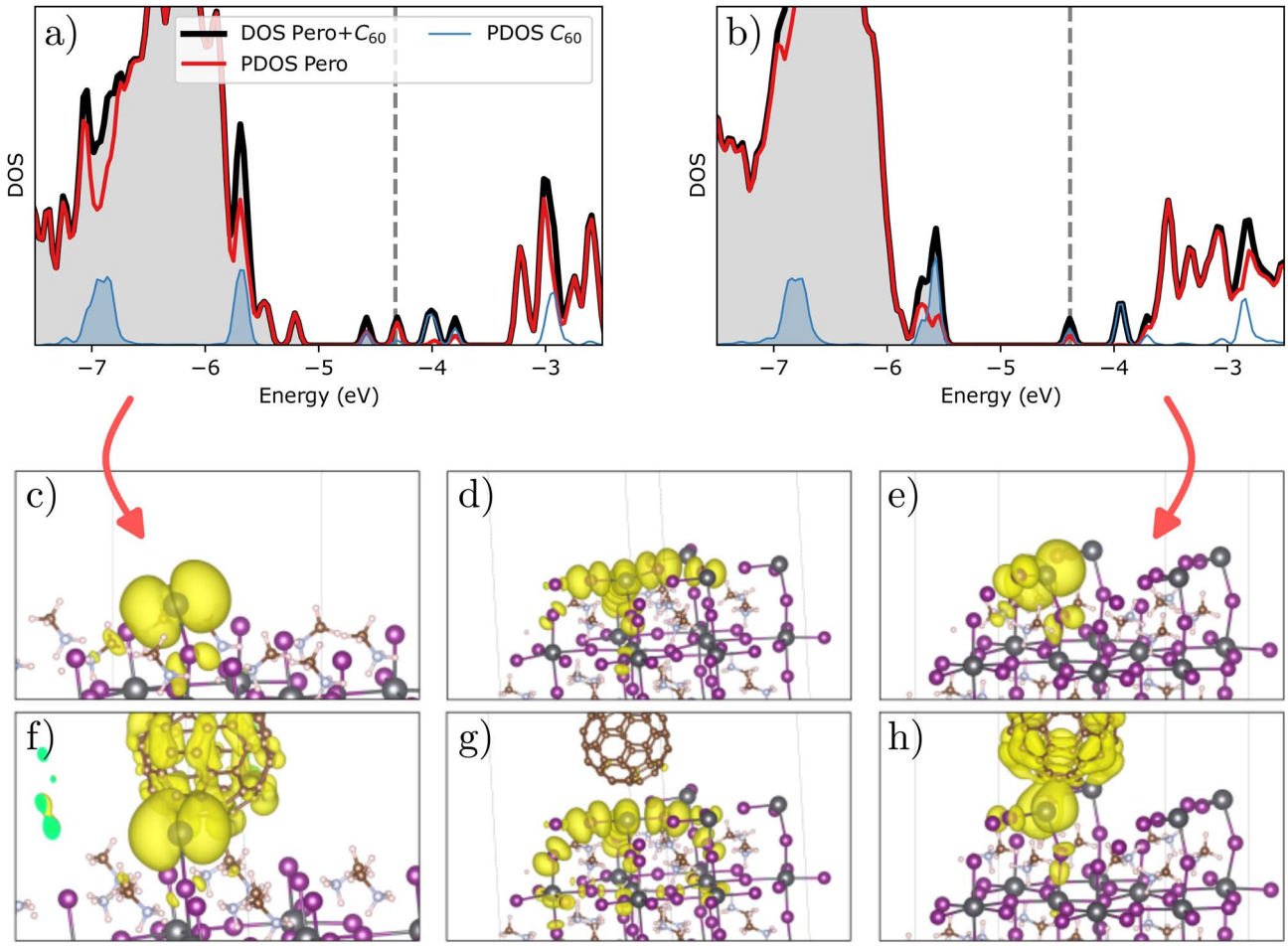

Fig. 4 Partial density of states at the PBE-level (a) and (b) for MAI:Pb_i and VAC:V_I showing midgap states with joint contribution of perovskite and C_{60}. Dashed grey line indicates the Fermi level. Projected contributions of selected defect orbitals to the charge density (also if not occupied) at the PBE-level are shown in (c) for MAI:Pb_i, (d) VAC:I_i and (e) VAC:V_I without C_{60} and (f) to (h) with C_{60}. Details about shown orbitals are discussed in SI VI.

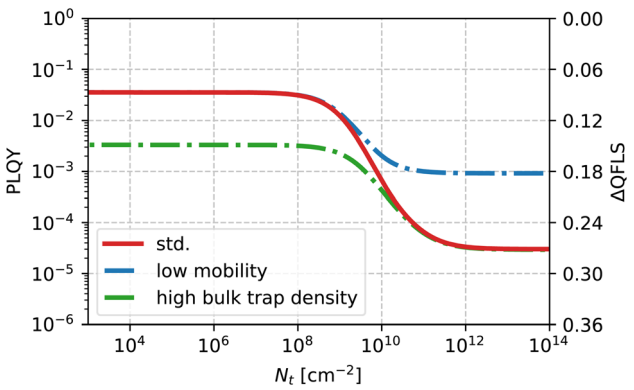

Fig. 5 Calculated PLQY and changes in QFLS as a function of surface trap density, for different scenarios: standard parameters (red); reduced perovskite mobility of 1 $cm^2 V^{-1} s^{-1}$ with all others parameters kept standard (blue); and increased bulk trap density of 3×10^{14} cm^{-3} with all other parameters in the standard configuration (green).

V_{OC} potential of the perovskite absorber, we calculated the PLQY of the perovskite absorber as a function of surface trap density, utilizing drift-diffusion simulations as detailed in the SI.

As shown in Fig. 5, we observe a decay in PLQY by three orders of magnitude beyond surface trap densities of 10^9 cm^{-2}. According to our HSE-level results, the presence of C_{60} could increase the density by two to three orders of magnitude, which would account for the entire PLQY reduction shown in Fig. 5, and our findings could indeed explain the PLQY decrease and the QFLS and V_{OC} reductions observed in the literature.[4,5,14–18]

Interestingly, we observe no further changes in the PLQY for densities larger than 10^{12} cm^{-2}, as the excess carriers are limited by their mobility in reaching the surface. A low mobility in the perovskite, observed *e.g.* in low-quality perovskite layers with small grain sizes,[19] is consequently less impacted by surface defects as revealed in Fig. 5 (blue line). Similarly, a high bulk trap density can lead to low PLQY values even without high surface defect density, again limiting the impact of additional surface defect. Together these highlight the importance of surface defect stability by C_{60} for high-quality perovskite layers and high-performance solar cells.

3.3. Strategies minimizing C_{60} induced recombination

The stabilization of defects in the vicinity of C_{60} highlights the importance of traditional strategies to minimize surface

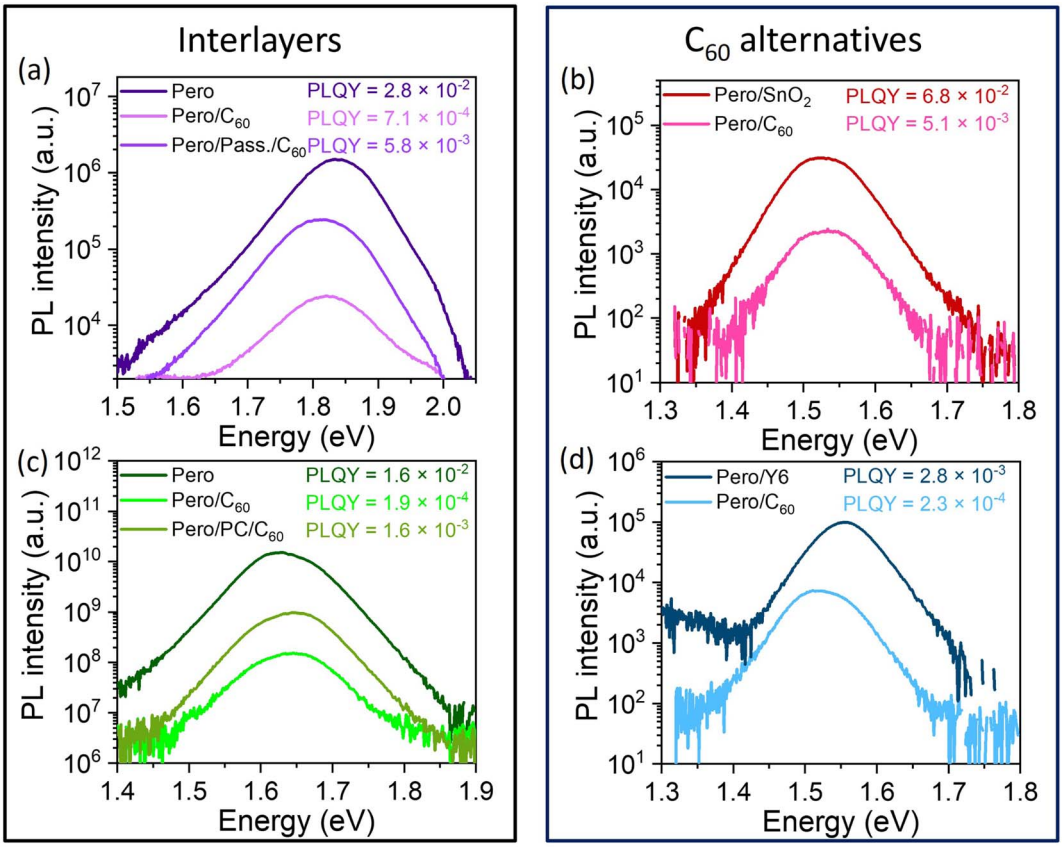

Fig. 6 Experimental PLQY values for perovskite films with different stacks. (a) *Cis*–$CyDAI_2$ as a passivation (Pass.) layer is applied at the perovskite/C_{60} interface[20] and (c) an insulating layer with apertures as a point contact (PC) layer.[22] (b) SnO_2 or (d) Y6 is applied as the ETL for perovskite, in comparison to C_{60}.

recombination at the perovskite/C_{60} interface. This is consistent with the less PL quenching when the *cis*-$CyDAI_2$ molecule[20] is utilized as a passivation (Pass.) layer between the perovskite and C_{60} layer, compared to the direct contact of perovskite with C_{60}, as shown in Fig. 6a. Furthermore, our results and insights provide new guidelines to circumvent these non-radiative recombination losses. A crucial fact is that the combination of the spherical shape of C_{60} with its pi-conjugated system ideally suits to overlap with defect orbitals, causing hybridization, regardless of its orientation. Future ETL materials should be chosen according to this criterion. Possible candidates would be suitable solid state materials, with delocalized conduction bands instead of localized LUMOs, *e.g.* TiO_2 or SnO_2. These materials are commonly used as ETL layers in n–i–p based perovskites solar cells, where their high temperature processing can be done prior to perovskite deposition, and indeed, Warby *et al.*[5] reported PLQY values close to those of neat perovskite layers for SnO_2. The use of SnO_2 nanoparticles, which circumvent high-temperature processing, has recently been extended to p–i–n based perovskite solar architectures.[21] The reduced non-radiative recombination with SnO_2 as the ETL is supported by the higher PLQY value, compared to that of C_{60}, as shown in Fig. 6b.

As an alternative, reducing the contact area of C_{60} with the perovskite through the use of an insulating interlayer with determined apertures can reduce the PL quenching induced by C_{60}, as shown in Fig. 6c, and therefore improve the device performance.[15,22] This approach, which is similar to point contacts employed in silicon solar cells,[23] requires a delicate compromise between surface coverage fraction and electron extraction efficiencies. Furthermore, electron conducting carboranes[10] that minimize defect stabilization could be an interesting strategy. Recently, non-fullerene acceptors such as Y6 and their derivatives have been utilized as ETLs in PSCs. A higher PLQY is observed with Y6 as the ETL, compared to C_{60}, which might be due to reduced defect stabilization.

4. Summary and conclusions

In summary, we have revealed an hitherto unknown mechanism for the stabilization of defects at a perovskite surface in the presence of C_{60}, causing an overall increased surface trap density, in case of a fully covered perovskite surface with C_{60} molecules. DFT calculations show that the underlying reason is the hybridization between the defect orbitals and the LUMO of C_{60}. The latter provides a pi-conjugated system, ideally suited to overlap with defect orbitals, causing hybridization. In other words, defects allow C_{60} not only to physisorb but also chemisorb, which in turn reduces the formation energy of the given defect. This finding can explain universally observed losses at

the perovskite/C_{60} interface and even the inverse proportionality of surface coverage and PLQY (see Warby *et al.*[5]): even a 1 nm thin C_{60} layer induces subgap states at the interface that completely quench the PLQY. Our results thus contribute significantly to a full understanding of the underlying mechanism of the problematic perovskite/C_{60} interface. With this work, we hope to shed new light on an important, yet poorly understood problem in the perovskite community, which impedes development of highly efficient perovskite single and multijunction photovoltaics.

Conflicts of interest

There are no conflicts to declare.

Data availability

The data, input files and crystal structures that support the findings of this work are available from the corresponding author under reasonable request. Ref. 24–34 are cited in the supplementary information (SI). Supplementary information is available. See DOI: https://doi.org/10.1039/d5el00161g.

Acknowledgements

The authors gratefully acknowledge the computing time made available for them on the high-performance computer "Lise" at the NHR Center NHR@ZIB. This center is jointly supported by the Federal Ministry of Education and Research and the state governments participating in the NHR (http://www.nhr-verein.de/unsere-partner). They also gratefully acknowledge the funding of this project by computing time provided by the Paderborn Center for Parallel Computing (PC2). F. L thanks the Volkswagen Foundation for funding *via* the Freigeist-Programme.

References

1 N. R. E. Laboratory, *Best Research-Cell Efficiency Chart*.
2 M. Stolterfoht, M. Grischek, P. Caprioglio, C. M. Wolff, E. Gutierrez-Partida, F. Peña-Camargo, D. Rothhardt, S. Zhang, M. Raoufi, J. Wolansky, M. Abdi-Jalebi, S. D. Stranks, S. Albrecht, T. Kirchartz and D. Neher, *Adv. Mater.*, 2020, **32**, 2000080), https://onlinelibrary.wiley.com/doi/pdf/10.1002/adma.202000080.
3 F. Lang, E. Köhnen, J. Warby, K. Xu, M. Grischek, P. Wagner, D. Neher, L. Korte, S. Albrecht and M. Stolterfoht, *ACS Energy Lett.*, 2021, **6**, 3982, DOI: 10.1021/acsenergylett.1c01783.
4 J. Thiesbrummel, F. Peña-Camargo, K. O. Brinkmann, E. Gutierrez-Partida, F. Yang, J. Warby, S. Albrecht, D. Neher, T. Riedl, H. J. Snaith, M. Stolterfoht and F. Lang, *Adv. Energy Mater.*, 2023, **13**, 2202674), https://advanced.onlinelibrary.wiley.com/doi/pdf/10.1002/aenm.202202674.
5 J. Warby, F. Zu, S. Zeiske, E. Gutierrez-Partida, L. Frohloff, S. Kahmann, K. Frohna, E. Mosconi, E. Radicchi, F. Lang, S. Shah, F. Peña-Camargo, H. Hempel, T. Unold, N. Koch, A. Armin, F. De Angelis, S. D. Stranks, D. Neher and M. Stolterfoht, *Adv. Energy Mater.*, 2022, **12**, 2103567), https://onlinelibrary.wiley.com/doi/pdf/10.1002/aenm.202103567.
6 G. Kresse and J. Furthmüller, *Phys. Rev. B:Condens. Matter Mater. Phys.*, 1996, **54**, 11169.
7 C. Quarti, F. De Angelis and D. Beljonne, *Chem. Mater.*, 2017, **29**, 958, DOI: 10.1021/acs.chemmater.6b03259.
8 J. Haruyama, K. Sodeyama, L. Han and Y. Tateyama, *J. Phys. Chem. Lett.*, 2014, **5**, 2903, DOI: 10.1021/jz501510v.
9 H. Uratani and K. Yamashita, *J. Phys. Chem. Lett.*, 2017, **8**, 742, DOI: 10.1021/acs.jpclett.7b00055.
10 F. Ye, S. Zhang, J. Warby, J. Wu, E. Gutierrez-Partida, F. Lang, S. Shah, E. Saglamkaya, B. Sun, F. Zu, S. Shoaee, H. Wang, B. Stiller, D. Neher, W.-H. Zhu, M. Stolterfoht and Y. Wu, *Nat. Commun.*, 2022, **13**, 7454.
11 C. C. Stoumpos, C. D. Malliakas and M. G. Kanatzidis, *Inorg. Chem.*, 2013, **52**, 9019, DOI: 10.1021/ic401215x.
12 K. Momma and F. Izumi, *J. Appl. Crystallogr.*, 2011, **44**, 1272.
13 C. Freysoldt, B. Grabowski, T. Hickel, J. Neugebauer, G. Kresse, A. Janotti and C. G. Van de Walle, *Rev. Mod. Phys.*, 2014, **86**, 253.
14 F. Ye, S. Zhang, F. Lang, M. Raoufi, J. Liang, I. Levine, H. Hempel, D. Menzel, F. Zu, S. Albrecht, L. Korte, C. Messmer, J. Schön, S. W. Glunz, T. Unold, N. Koch, D. Neher, D. Ye, Y. Wu and M. Stolterfoht, *ACS Energy Lett.*, 2025, **10**, 2942, DOI: 10.1021/acsenergylett.5c00615.
15 G. He, A.-F. Castro-Méndez, J. Diekmann, G. J. W. Aalbers, P. Forozi Sowmeeh, A. Singh, S. V. Quiroz Monnens, F. Peña-Camargo, M. Stolterfoht, B. Stannowski, H. C. Neitzert, R. A. J. Janssen, C. M. Wolff, D. Neher and F. Lang, *EES Sol.*, 2025, **1**(5), 775–785.
16 X. Jiang, S. Qin, L. Meng, G. He, J. Zhang, Y. Wang, Y. Zhu, T. Zou, Y. Gong, Z. Chen, G. Sun, M. Liu, X. Li, F. Lang and Y. Li, *Nature*, 2024, **635**, 860.
17 F. Yang, P. Tockhorn, A. Musiienko, F. Lang, D. Menzel, R. Macqueen, E. Köhnen, K. Xu, S. Mariotti, D. Mantione, L. Merten, A. Hinderhofer, B. Li, D. R. Wargulski, S. P. Harvey, J. Zhang, F. Scheler, S. Berwig, M. Roß, J. Thiesbrummel, A. Al-Ashouri, K. O. Brinkmann, T. Riedl, F. Schreiber, D. Abou-Ras, H. Snaith, D. Neher, L. Korte, M. Stolterfoht and S. Albrecht, *Adv. Mater.*, 2024, **36**, 2307743), https://advanced.onlinelibrary.wiley.com/doi/pdf/10.1002/adma.202307743.
18 R. He, W. Wang, Z. Yi, F. Lang, C. Chen, J. Luo, J. Zhu, J. Thiesbrummel, S. Shah, K. Wei, Y. Luo, C. Wang, H. Lai, H. Huang, J. Zhou, B. Zou, X. Yin, S. Ren, X. Hao, L. Wu, J. Zhang, J. Zhang, M. Stolterfoht, F. Fu, W. Tang and D. Zhao, *Nature*, 2023, **618**, 80.
19 O. Shargaieva, F. Lang, J. Rappich, T. Dittrich, M. Klaus, M. Meixner, C. Genzel and N. H. Nickel, *ACS Appl. Mater. Interfaces*, 2017, **9**, 38428, DOI: 10.1021/acsami.7b10056.
20 X. Jiang, S. Qin, L. Meng, G. He, J. Zhang, Y. Wang, Y. Zhu, T. Zou, Y. Gong, Z. Chen, G. Sun, M. Liu, X. Li, F. Lang and Y. Li, *Nature*, 2024, **635**, 860.
21 S. Y. Kim, M. Y. Woo, M. J. Jeong, S. W. Jeon, J. W. Ahn, J. H. Park, C. Y. Kim, D. H. Kim, O. J. Oh, G. Yu, S. Lee, C. Kim, D. H. Kim and J. H. Noh, *Adv. Energy Mater.*, 2024,

14, 2402433), https://advanced.onlinelibrary.wiley.com/doi/pdf/10.1002/aenm.202402433.

22 K. Mao, F. Cai, Z. Zhu, H. Meng, T. Li, S. Yuan, J. Zhang, W. Peng, J. Xu, X. Feng, Q. Chen and J. Xu, *Adv. Energy Mater.*, 2023, **13**, 2302132), https://advanced.onlinelibrary.wiley.com/doi/pdf/10.1002/aenm.202302132.

23 A. W. Blakers, A. Wang, A. M. Milne, J. Zhao and M. A. Green, *Appl. Phys. Lett.*, 1989, **55**, 1363), https://pubs.aip.org/aip/apl/article-pdf/55/13/1363/18473099/1363_1_online.pdf.

24 P. E. Blöchl, *Phys. Rev. B:Condens. Matter Mater. Phys.*, 1994, **50**, 17953.

25 J. P. Perdew, K. Burke and M. Ernzerhof, *Phys. Rev. Lett.*, 1996, **77**, 3865.

26 J. Heyd, G. E. Scuseria and M. Ernzerhof, *J. Chem. Phys.*, 2006, **124**, 219906), https://pubs.aip.org/aip/jcp/article-pdf/doi/10.1063/1.2204597/15387022/219906_1_online.pdf.

27 M.-H. Du, *J. Phys. Chem. Lett.*, 2015, **6**, 1461, DOI: 10.1021/acs.jpclett.5b00199.

28 S. Grimme, J. Antony, S. Ehrlich and H. Krieg, *J. Chem. Phys.*, 2010, **132**, 154104), https://pubs.aip.org/aip/jcp/article-pdf/doi/10.1063/1.3382344/15684000/154104_1_online.pdf.

29 U. Aeberhard, S. Altazin, L. Stepanova, A. Stous, B. Blülle, C. Kirsch, E. Knapp and B. Ruhstaller, in *2019 IEEE 46th Photovoltaic Specialists Conference (PVSC)*, 2019, pp. 0105–0111.

30 J. Diekmann, P. Caprioglio, M. H. Futscher, V. M. Le Corre, S. Reichert, F. Jaiser, M. Arvind, L. P. Toro, E. Gutierrez-Partida, F. Peña-Camargo, C. Deibel, B. Ehrler, T. Unold, T. Kirchartz, D. Neher and M. Stolterfoht, *Sol. RRL*, 2021, **5**, 2100219), https://onlinelibrary.wiley.com/doi/pdf/10.1002/solr.202100219.

31 A. Al-Ashouri, E. Köhnen, B. Li, A. Magomedov, H. Hempel, P. Caprioglio, J. A. Márquez, A. B. M. Vilches, E. Kasparavicius, J. A. Smith, N. Phung, D. Menzel, M. Grischek, L. Kegelmann, D. Skroblin, C. Gollwitzer, T. Malinauskas, M. Jošt, G. Matič, B. Rech, R. Schlatmann, M. Topič, L. Korte, A. Abate, B. Stannowski, D. Neher, M. Stolterfoht, T. Unold, V. Getautis and S. Albrecht, *Science*, 2020, **370**, 1300), https://www.science.org/doi/pdf/10.1126/science.abd4016.

32 L. M. Herz, *ACS Energy Lett.*, 2017, **2**, 1539, DOI: 10.1021/acsenergylett.7b00276.

33 X. Zhang, M. E. Turiansky, J.-X. Shen and C. G. Van de Walle, *Phys. Rev. B*, 2020, **101**, 140101.

34 D. Meggiolaro, S. G. Motti, E. Mosconi, A. J. Barker, J. Ball, C. Andrea Riccardo Perini, F. Deschler, A. Petrozza and F. De Angelis, *Energy Environ. Sci.*, 2018, **11**, 702.